ACS APPLIED MATERIALS & INTERFACES

Letter

www.acsami.org

Enhanced Electrical and Mechanical Properties of Silver Nanoplatelet-Based Conductive Features Direct Printed on a Flexible Substrate

Young-In Lee,[†] Seil Kim,[‡] Seung-Boo Jung,[§] Nosang V. Myung,[†] and Yong-Ho Choa*[,‡]

[†]Department of Chemical and Environmental Engineering and Center for Nanoscale Science and Engineering, University of California-Riverside, Riverside, California 92521, United States

[‡]Department of Bionano Technology, Hanyang University, Ansan 426-791, Republic of Korea

[§]School of Advanced Materials Science and Engineering, Sungkyunkwan University, Suwon 440-476, Republic of Korea

Supporting Information

ABSTRACT: Noncontact direct printed conductive silver patterns with an enhanced flexural and bending strength and a proper electrical resistivity were fabricated using silver nanoplatelet inks without any surfactants for particle dispersion on a polyimide film. The microstructure, electrical resistivity, and bending strength of conductive features based on the nanoplatelets are systematically investigated and compared to nanoparticles to demonstrate superior properties. Nanoplatelets stack neatly on the substrate after noncontact direct printing, which minimizes void formation during sintering. This microstructure results in excellent resistivity on external repetitive bending stress as well as sufficiently lower electrical resistivity. It is believed to be a general conductive material to fabricate the noncontact direct printed conductive patterns with excellent mechanical stability for various flexible electronics, including solar cells, displays, RFID, and sensors.

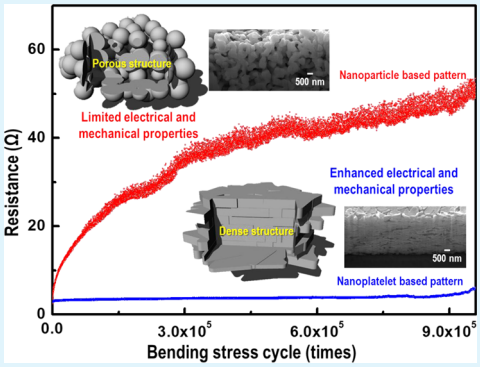

KEYWORDS: *silver nanoplatelets, direct printing, flexible substrates, conductive features, mechanical properties*

INTRODUCTION

Direct printing methods, including dispenser,[1,2] gravure,[3,4] flexography,[5] and inkjet[6−8] printing, have been intensively investigated as low-cost "greener" alternatives to traditional subtractive photolithography to create electrical connections. In addition, these methods can write directly on various substrates (i.e., polyimide, polyethylene terephthalate, polycarbonate, and paper)[9−12] to form flexible electronics including displays,[13] solar cell arrays,[14] radio frequency identification (RFID) tags,[15] and chemical sensors.[16] These applications require electrical contacts with excellent electrical conductance and mechanical properties. Direct printing methods generally create conductive features from ink or paste containing metals, such as micrometer or nanoparticles. Conductive features printed on flexible substrate should be electrically conductive, resist repetitive bending stress, and be properly adhered to substrates. The electrical conductivity and mechanical properties are determined by a conductive medium's sinterability and packability during low temperature sintering and affect its composition, shape, morphology, size, and distribution.[34]

Currently, most research on conductive patterns printed directly on flexible substrates has been focused on enhancing electrical conductivity by controlling the diameter of conductive particles while decreasing the sintering temperature because of thermal compatibility.[17−20] Although nanoparticles with a high surface area to volume ratio improved the electrical properties, converting a layer of nanoparticles into a fully densified film or line without applying high pressure is still difficult because the higher surface area to volume leads to particles agglomerating and trapping gases on the surface.[21] Therefore, it is necessary to use dispersion agents that could inhibit the decrease in stability by coating dispersion agent on the surfaces of the nanoparticles.[22,23] However, these dispersion agents generally have high molecular weights. Thus, a high temperature was demanded to decompose such heavy molecular materials, which hinder the application of metal nanoparticle based ink on flexible substrates. In addition, at low temperature and moderate pressure, the mass flow to minimize Gibbs free energy mainly occurs at the particle surface, causing neck growth without changing particle spacing (no shrinkage or densification). Thus, fully eliminating the void between particles during sintering is impossible. Therefore, directly printing nanoparticles results in porous structures, which lead to lower conductivity and poor mechanical resistibility to external stress compared to electrochemical and physical vapor deposited patterns. This problem is more significant in noncontact direct printing, such as dispenser, aerosolized jet, inkjet, and spray coating because the only external force to

Received: May 9, 2013
Accepted: June 20, 2013
Published: June 20, 2013

increase the packing density of conductive materials during printing is gravity. Thus, developing nanoengineered materials that form dense conductive features with enhanced electrical conductivity and flexural and adhesion strength by increasing the packing density is essential.

One way to solve this problem is using nanoplatelets instead of nanoparticles. Metallic platelets with a micrometre scale are used in various applications, including conductive adhesives, internal multilayer ceramic capacitor electrodes, and solar cells because they do not easily agglomerate, allowing them to form conductive features with high packing densities. To use the metallic platelets as a conductive material for conductive patterns printed on flexible substrates, the platelet dimensions, including thickness, need to be optimized to nanometre scale to secure sinterability as well as packing density. To the best of our knowledge, no reports have been used metallic nanoplatelets to form conductive features on a flexible substrate.

Herein, we fabricated direct printed conductive features with superior flexural strength on a flexible substrate as well as a proper electrical resistivity using silver nanoplatelet based inks without any surfactants for particle dispersion. Silver was selected as the conductive material because of its high conductivity and resistance to oxidation. In addition, the synthesis of silver nanoplatelets with a controlled shape, morphology, and dimensions has been previously reported.[24−26] The microstructure, electrical conductivity, and bending and adhesion strength of conductive features based on nanoplatelets were systematically investigated and compared to conductive features based on nanoparticles to demonstrate superior properties.

EXPERIMENTAL PROCEDURE

Silver nanoplatelets were synthesized by solvothermal process that has been described in detail previously.[27] Poly(vinyl pyrrolidione) (PVP, MW = 29 000, Sigma-Aldrich) was added to N,N-dimethylformamide (DMF, > 99.8%, Sigma-Aldrich) in a beaker, and mixed until completely dissolved. Silver nitrate (50 mM $AgNO_3$, > 99%, Junsei) was rapidly added to the solution. After the $AgNO_3$ had completely dissolved, the solution was quickly transferred to a benchtop reactor (Model 4843, Parr Instrument Company) at 160 °C. After incubating for 4 h, samples were collected, centrifuged, and washed with water many times to remove the solution and excess PVP.

The synthesized silver nanoplatelets and commercial silver nanopowders (<100 nm, Sigma Aldrich) were used as materials to form conductive features on a flexible substrate. They were added and ultrasonically dispersed in ethanol to 20 wt % without any dispersion agents for printing inks. The ink viscosity was characterized with a viscometer (LVDV-II + CP, Brookfield Inc.). Various conductive patterns were formed on polyimide film (Kolon LV 200, 50 um thickness) using dispenser printing system (SMP-III, RichStone Ltd.) composed of a syringe and needle connected to a plunger controller. The ink was loaded into a 5 mL plastic syringe connected to a nozzle with a capillary tip (0.2 mm diameter). The nozzle ejected droplets of a constant volume of 0.5 μL on the polyimide film to fabricate patterns. The nozzle to surface distance was set to 5 mm. The printed patterns were annealed at 200 °C for 1 h in ambient atmosphere.

Transmission electron microscopy (TEM, JEOL JEM-2100F) and atomic force microscopy (AFM; XE 100, PSIA) were used to analyze the morphology and microstructure of silver nanoplatelets. X-ray diffractometry (XRD; Rigaku, CuKα) was carried out to confirm the crystal structure of the patterns. The pattern microstructures were investigated by field emission scanning electron microscopy (FE-SEM; Hitachi S-4800) and focus ion beam equipped SEM (FIB; Tescan LYRA 1 FEG). In addition, the resistivity was measured using sheet resistance obtained by a four-point probe (ATI CMT-SR2000N) and the pattern thickness. To evaluate the mechanical properties of printed silver patterns, we tested the IPC flexural resistance endurance using the IPC sliding tester (Ajeontech, Korea). Figure S1 in the Supporting Information shows illustrations and images of a test sample (15 mm wide, 150 mm long) and the machine. The sample was loaded into the system halfway and the gap between the upper and lower samples was set to 5 mm. The lower plate moved forward and backward with a 25 mm stroke at 170 cycles/min, and the resistance of the silver pattern was measured at the same time. The test was carried out for 959,140 cycles and the changes to the microstructure were observed by FE-SEM after the test.

RESULTS AND DISCUSSION

The silver nanoplatelets used to create conductive patterns were synthesized by a mass-productive, rapid, and simple solvothermal solution approach. The shape, size, and morphology of silver nanoplatelets can be controlled by modulating factors such as reaction time, reactant concentrations, and reaction temperature. Images A and B in Figure 1

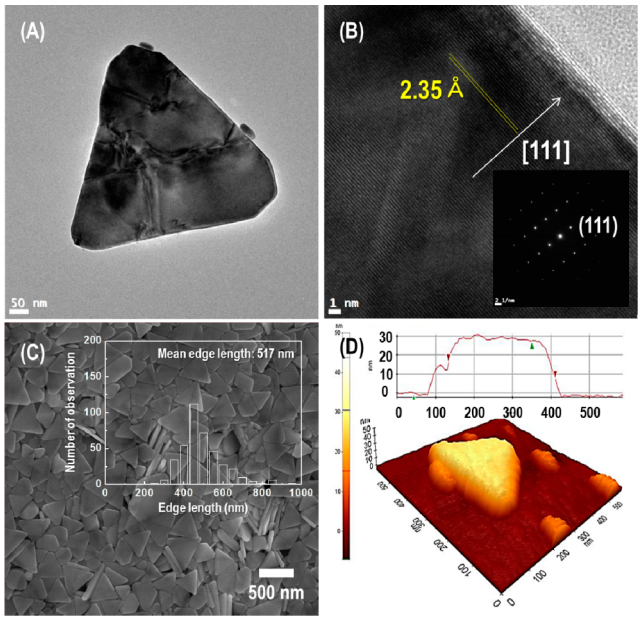

Figure 1. (A) TEM image, (B) high-resolution TEM images with SAED patterns (inset image), (C) FE-SEM image with edge length distribution (inset graph) and (D) AFM image and thickness profile of silver nanoplatelets synthesized by solvothermal method.

show a single triangular plate that has an edge length of approximately 530 nm and good crystallinity. The fringes at the edge of Figure 1B are separated by 2.35 Å, which can be ascribed to (111) reflection. The inset in Figure 1B shows a typical selected area diffraction pattern, and the spot points clearly indicate that the platelet is a single crystal with its [111] orientation parallel to the electron beam. The XRD pattern of solvothermally synthesized nanoplatelets shown in Figure 3 (B) also demonstrates that the basal plane (i.e., the top crystal plane

dx.doi.org/10.1021/am401757y | ACS Appl. Mater. Interfaces 2013, 5, 5908−5913

of the nanoplates) is the (111) plane because the overwhelmingly intensive diffraction peak was located at 2θ = 38.06°, which is from the (111) lattice plane of face-centered cubic (fcc) silver. Figure 1C shows a FE-SEM image and edge length distributions of silver nanoplatelets synthesized by the solvothermal method. The synthesized silver nanoplatelets were triangular and the narrow edge length distribution and average was approximately 517 nm. The nanoplatelets were approximately 30 nm thick by AFM analysis, shown in Figure 1D.

Two inks containing silver nanoplatelets or nanoparticles were directly printed to a square shape (2 cm × 2 cm) on polyimide (PI) films using a dispenser printing system. The viscosities of the silver nanoplatelet and nanoparticle based inks were 5.8 and 5.7 cP, respectively. The surface microstructures of silver patterns from the noncontact direct printing with different conductive materials and prepared by annealing at 200 °C in an ambient atmosphere for 1 h are shown in images A and B in Figure 2. The conductive patterns had clearly different

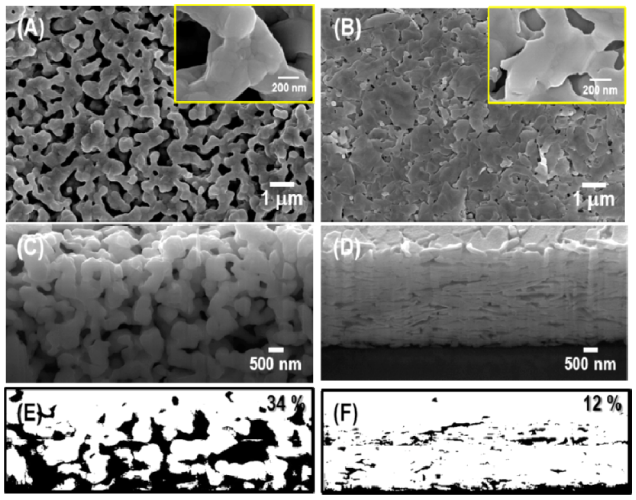

Figure 2. FE-SEM images showing the (A, B) surface and (C, D) cross-section microstructures and directly printed conductive patterns using (A, C, E) silver nanoparticles and (B, D, F) nanoplatelets after sintering at 200 °C for 1 h in air. (E, F) show the pore (black) and dense (white) areas.

microstructures depending on the precursor morphology. Patterns based on silver nanoparticles had a significantly higher void volume compared to patterns based on silver nanoplatelets. This result directly indicates the effect of conductive material morphology on the microstructure of conducting pattern after sintering. Although fractional density of monosized sphere is between 0.60 and 0.64, the actual density depends on the powder characteristics, namely the size and shape.[28] In theory, cube or cuboid particles can be packed up to 100% if arranged properly. The images in Figure 2 are consistent with this idea. The cross-sectional FE-SEM images also reveal that the microstructure of annealed patterns depended on the shape of the conductive material (Figure 2C, D). For silver nanoparticles Figure 2C, the cross-sectional image and surface morphologies were the same. On the contrary, silver nanoplatelets stacked neatly on the substrate with greater packing density (Figure 2D). Panels E and F in Figure 2 show the pore as black and dense areas as white colors. From these images, an image analysis program was used to calculate the pore volume. The porosities were approximately 34% for nanoparticles and 12% for nanoplatelets. The particle agglomeration could also affect the microstructures of the patterns because there are no surfactants for particle dispersion in the inks. The nanoplatelets are more stable against the agglomeration than the nanoparticles because of their small specific surface area (nanoplatelets: 3.83 m^2/g, nanoparticles: 6.96 m^2/g) and platelet morphology. As shown in Figure S2 in the Supporting Information, the printed pattern using the silver nanoparticle indicated agglomerated nanoparticles and a lot of voids, whereas the nanoplatelet was free of the agglomeration and the microstructure of the printed film is more compact.

Figure 3 shows XRD patterns for nanoparticles (Figure 3A) and nanoplatelets (Figure 3B) annealed at different temper-

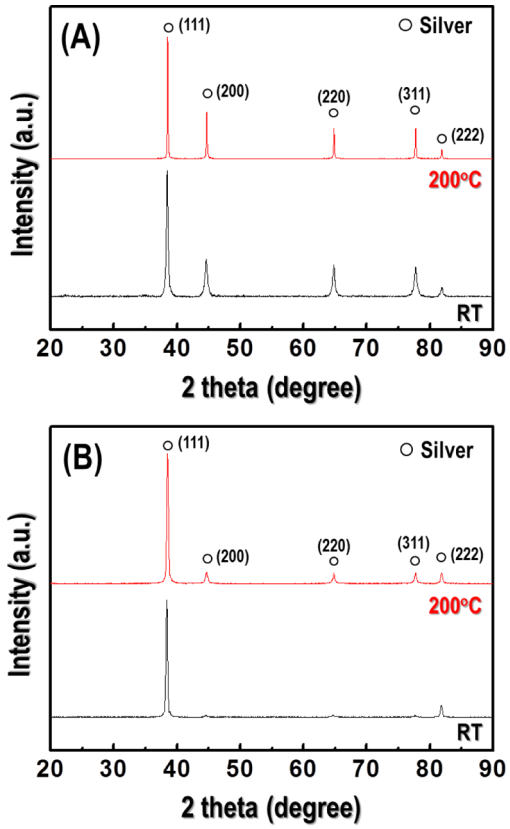

Figure 3. XRD patterns of directly printed patterns using (A) silver nanoparticles and (B) nanoplatelets before and after heat treatment at 200 °C for 1 h in air.

atures (200 and 300 °C) in an ambient atmosphere for 1 h. Five diffraction peaks were identified as the (111), (200), (220), (311), and (222) planes of face-centered cubic silver in all samples. These results indicated that there were no any secondary phases in the product. For nanoplatelets, the ratio between the intensities of (111) and (200) diffraction peaks was much higher than for commercial nanoparticles and a standard reference (in JCPDS) [(111)/(200) = 125 (nanoplatelets), 3.52 (nanoparticles), and 2.15 (JCDPS card #65–2871)], which is consistent with the preferred (111) facets. These XRD patterns show that (111) plane in silver nanoplatelets oriented parallel to the supporting substrate after printing. If the nanoplatelets do not arrange uniformly with the substrate, all peak intensities except (111) should increase. This phenomenon will allow for highly dense patterns.

dx.doi.org/10.1021/am401757y | ACS Appl. Mater. Interfaces 2013, 5, 5908–5913

Table 1. Comparison of the Electrical Resistivity of Direct Printed Silver Patterns[a]

		curing				
materials	avg particle size (nm)	temp./time (°C/ min)	heating rate (°C/min)	surfactant	lowest resistivity ($\mu\Omega$ cm)	ref
Ag NPs	2.1	200/60	10	EG	6.8	31
Ag NPs	50	260/3		PVP	16	32
Ag NPs	40	180/60	2	polymer	5	20
Ag NPs	20	250/90	10	poly(acrylic acid)	52	19
Ag NPs	20	160/30		PVP	8.8	33
Ag NPs	100	200/60	10	none	30 ± 3.65	this work
Ag NTs	E:518, T:30	200/60	10	none	7.4 ± 0.65	this work

[a]NPs, nanoparticles; NTs, nanoplatelets; E, edge; T, thickness; EG, ethylene glycol; PVP, polyvinylpyrrolidone.

The preferred stack orientation of silver nanoplatelets in the pattern remained after sintering.

The pattern microstructure strongly influenced the electrical conductivity and flexural strength of the pattern. Table 1 shows the specific electrical resistances of silver patterns fabricated using silver nanoplatelets and nanoparticles in this study and the comparison with those of direct printed silver patterns previously reported. Nanoplatelet patterns sintered at 200 °C had the resistivity of average 7.4 $\mu\Omega$ cm (bulk silver resistivity: 1.59 $\mu\Omega$ cm). This value has significantly lower electrical resistivity than that of nanoparticles based patterns (30 $\mu\Omega$ cm). This result clearly shows that the electrical resistivity is functionally related to the pattern microstructure. It is clearly observed that necks between the nanoplatelets are well formed after sintering, which allows a percolation path for the electricity. Although the nanoparticles also show well-sintered structures, they have a lot of pores in the microstructure. The pores in the sintered conductive pattern may reduce the number of the percolation pathways.[29,30] Therefore, the electrical resistivity of the pattern based on the nanoplatelets was enhanced than that of nanoparticles because of higher packing density as shown in Figure 2. Table 1 summarizes the operating parameters and the resistivity of prior works on direct printed silver patterns using silver nanoparticle based inks and this work. The resistivity of the conductive pattern typically depends on several factors, including the diameter of conductive media, a sintering temperature and time, a ramping rate for sintering, and surfactants for dispersion.[20,35−37] The nanoparticle-based pattern in this work exhibits a high resistivity compared with the referred results because the pattern was fabricated by relatively large nanoparticles without any surfactants for a dispersion. In the case of the nanoplatelet, the specific surface area of the nanoplatelets is much smaller than the nanoparticles as mentioned above, however, the printed nanoplatelet pattern had a similar or lower resistivity compared with the prior works resulting from its compact microstructure. Figures S3 and S4 in the Supporting Information shows the resistivity and FE-SEM images of silver patterns as a function of sintering temperature. The both films show a drastic decrease in resistivity between 150 and 200 °C and an additional slight decrease above 200 °C. As shown in Figure S4 in the Supporting Information, the patterns that sintered at relatively high temperature show a well-sintered microstructure with larger grains because the driving force for the sintering increased. The development of microstructure are consistent with the decrease in resistivity shown in Figure S3 in the Supporting Information. The driving force can be also increased by decreasing the size of the conductive medium. Unfortunately, we did not investigate an effect of the nanoplatelet dimension and thickness on the pattern resistivity and microstructure in this study, it is expected to achieve a more densely compact and well-developed microstructure and a lower resistivity at a comparatively low sintering temperature if nanoplatelets with a smaller dimension and thickness are used.

The mechanical stability of electrical circuits printed directly on a flexible substrate during external strain is one of the most important factors for flexible electronics. Figure 4 shows the variations in resistance of nanoparticle and nanoplatelet patterns under repetitive bending stress. Nanoparticle and nanoplatelet patterns differed markedly. For a nanoparticle pattern with a thickness of about 5.9 μm, the initial resistance was 2.47 Ω and it increased rapidly to 51.45 Ω after 959 140 bending cycles. The rate of resistance increase was about 2,080% and in case of a thinner film of 4.1 μm, the resistance change rate is about 2160% (initial resistance = 2.54 Ω, after 959,140 cycle = 54.88 Ω), which is similar to that of 5.9 μm film. Cracks that easily formed in the pattern by bending stress likely degraded the electrical properties because the resistance

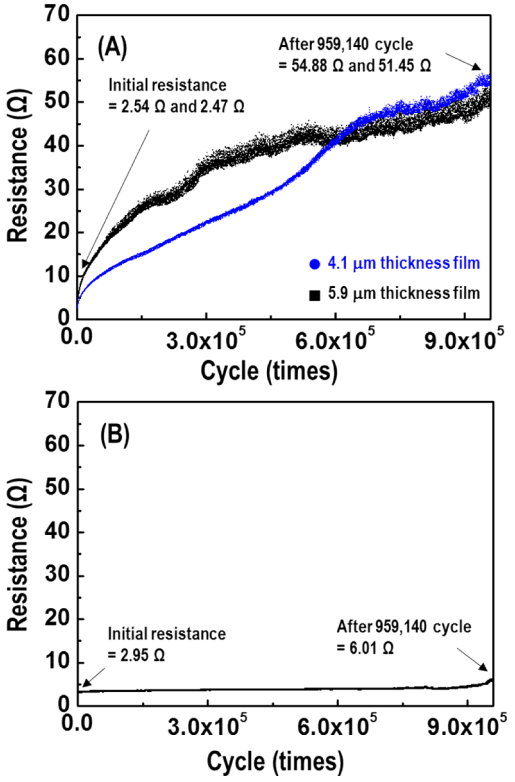

Figure 4. Graphs showing resistance variation of conductive patterns formed by (A) silver nanoparticles and (B) silver nanoplatelets at 200 °C under repetitive bending stress.

dx.doi.org/10.1021/am401757y | ACS Appl. Mater. Interfaces 2013, 5, 5908−5913

sharply increased throughout the test. In contrast, the electrical resistance of nanoplatelet patterns shows a small change rate as shown in Figure 4B. The result on the nanoplatelet patterns with a thickness of 3.3 μm was constant in the entire bending cycles except for the small increase in the resistance after the 900 000th cycle. The resistance increased a mere 200% from 2.95 to 6.01 Ω after 959 140 bending cycles. Therefore, the resistance change due to repetitive bending stress is connected to the microstructures. The silver nanoparticle patterns have to be vulnerable to bending stress because the many pores crack and move easily, thus the electrical resistivity increased sharply after bending stress. The dense microstructure of nanoplatelet patterns, however, withstood the bending stress by minimizing cracking and movement.

Figure 5 shows the microstructure of silver patterns after inducing repetitive bending stress. Many cracks about 50 μm

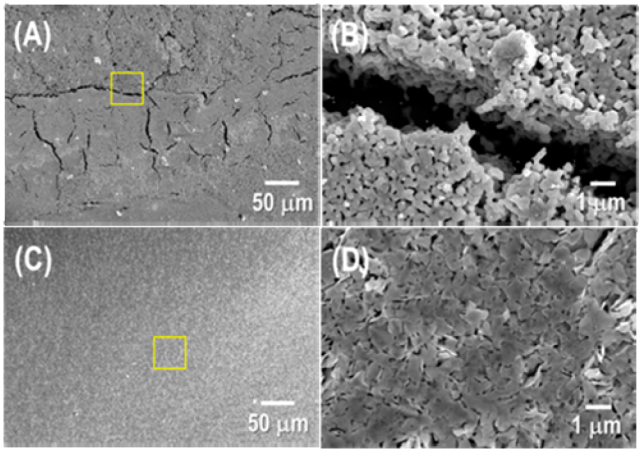

Figure 5. FE-SEM images showing the pattern microstructures made of (A, B) silver nanoparticles and (C, D) silver nanoplatelets at 200 °C after 959 140 bending cycles.

long were observed throughout the silver nanoparticle patterns. On the other hand, cracks of nanoplatelet patterns were difficult to find. Images show that crack formation likely causes the resistance increases (Figure 4), and cracks are minimized by using nanoplatelets. The mechanical stability test and FE-SEM images indicate that nanoplatelet patterns with dense microstructure have excellent resistivity on repetitive bending stress compared with nanoparticles.

CONCLUSIONS

In conclusion, we demonstrated highly dense conductive patterns with excellent electrical and mechanical properties using silver nanoplatelets as the conductive materials. Nanoplatelets stack neatly on the substrate after direct printing, which minimizes void formation. The direct printed nanoplatelets have significantly lower electrical resistivity than nanoparticles (7.4 $\mu\Omega$ cm compared to 30 $\mu\Omega$ cm). In addition, nanoplatelet-based conductive patterns have excellent stability on external repetitive bending stress because they do not crack upon external bending stress. Improved electrical resistivity and mechanical stability can be attributed to the dense microstructure resulting nanoplatelet conductive material. These findings can be readily applied to various flexible electronics, including solar cells, displays, RFID, and sensors.

ASSOCIATED CONTENT

Supporting Information

Illustrations of the IPC flexural resistance endurance test machine and sample, real optical images of direct printed Ag pattern, FE-SEM images of the Ag patterns before sintering, and resistivity and FE-SEM images as a function of sintering temperature. This material is available free of charge via the Internet at http://pubs.acs.org.

AUTHOR INFORMATION

Corresponding Author

*E-mail: choa15@hanyang.ac.kr. Tel.:+82-31-400-5650. Fax: +82-31-418-6490.

Notes

The authors declare no competing financial interest.

ACKNOWLEDGMENTS

This work was supported by a grant from the Fundamental R&D Program for Core Technology of Materials and the Energy Efficiency & Resources program of the Korea Institute of Energy Technology Evaluation and Planning (KETEP) grant funded by the Ministry of Knowledge Economy, Republic of Korea (20112010100100).

REFERENCES

(1) Ho, C. C.; Evans, J. W.; Wright, P. K. *J. Micromech. Microeng.* **2010**, *20*, 104009.
(2) Kuhn, M.; Napporn, T.; Meunier, M.; Vengallatore, S.; Therriault, D. *J. Micromech. Microeng.* **2008**, *18*, 015005.
(3) Puetz, J.; Aegeter, M. A. *Thin Solid Films* **2008**, *516*, 4495−4501.
(4) Voigt, M. M.; Guite, A.; Chung, D.-Y.; Khan, R. U. A.; Campbell, A. J.; Bradley, D. D. C.; Meng, F.; Steinke, J. H. G.; Tierney, S.; McCulloch, I.; Penxten, H.; Lutsen, L.; Douheret, O.; Manca, J.; Brokmann, U.; Sonnichsen, K.; Hulsenberg, D.; Bock, W.; Barron, C.; Blanckaert, N.; Springer, S.; Grupp, J.; Mosley, A. *Adv. Funct. Mater.* **2010**, *20*, 239−246.
(5) Huebner, C. F.; Carroll, J. B.; Evanoff, D. D.; Ying, Y.; Stevenson, B. J.; Lawrence, J. R.; Houchins, J. M.; Foguth, A. L.; Sperryb, J.; Foulge, S. H. *J. Mater. Chem.* **2008**, *18*, 4942−4948.
(6) Singh, M.; Haverinen, H. M.; Dhagat, P.; Jabbour, G. E. *Adv. Mater.* **2010**, *22*, 673−685.
(7) Minemawari, H.; Yamada, T.; Matsui, H.; Tsutsumi, J.; Haas, S.; Chiba, R.; Kumai1, R.; Hasegawa, T. *Nature* **2011**, *475*, 364−367.
(8) Vaseem, M.; Lee, K. M.; Hong, A.-R.; Hahn, Y.-B. *ACS Appl. Mater. Interfaces* **2012**, *4*, 3300−3307.
(9) Jang, S.; Seo, Y.; Choi, J.; Kim, T.; Cho, J.; Kim, S.; Kim, D. *Scr. Mater.* **2010**, *62*, 258−261.
(10) Osch, T. H. J.; Perelaer, J.; Laat, A. W. M.; Schubert, U. S. *Adv. Mater.* **2008**, *20*, 343−345.
(11) Perelaer, J.; Hendriks, C. E.; Laat, A. W. M.; Schubert, U. S. *Nanotechnology* **2009**, *20*, 165303.
(12) Siegel, C.; Phillips, S, T.; Dickey, , M, D.; Lu, , N.; Suo, , Z.; Whitesides, , G. M. *Adv. Funct. Mater.* **2010**, *20*, 28−35.
(13) Chen, Y.; Au, J.; Kazlas, P.; Ritenour, A.; Gates, H.; McCreary, M. *Nature* **2003**, *423*, 136.
(14) Krebs, F. C.; Jørgensen, M.; Norrman, K.; Hagemann, O.; Alstrup, J.; Nielsen, T. D.; Fyenbo, J.; Larsen, K.; Kristensen, J. *Sol. Energy Mater. Sol. Cells* **2009**, *93*, 422−441.
(15) Komoda, N.; Nogi, M.; Suganuma, K.; Otsuka, K. *ACS Appl. Mater. Interfaces* **2012**, *4*, 5732−5736.
(16) Dua, V.; Surwade, S. P.; Ammu, S.; Agnihotra, S. R.; Jain, S.; Roberts, K. E.; Park, S.; Ruoff, R. S.; Manohar, S. K. *Angew. Chem., Int. Ed.* **2010**, *49*, 2154−2157.
(17) Lee, Y.; Choi, J.; Lee, K. J.; Stott, N. E.; Kim, D. *Nanotechnology* **2008**, *19*, 415604.

(18) Grouchko, M.; Kamyshny, A.; Magdassi, S. *J. Mater. Chem.* **2009**, *19*, 3057−3062.
(19) Ahn, B. Y.; Duoss, E. B.; Motala, M. J.; Guo, X.; Park, S.-I.; Xiong, Y.; Yoon, J.; Nuzzo, R. G.; Rogers, J. A.; Lewis, J. A. *Science* **2009**, *323*, 1590−1593.
(20) Greer, J. R.; Street, R. A. *Acta Mater.* **2007**, *55*, 6345−6349.
(21) Jung, J.; Kang, S. *J. Am. Ceram. Soc.* **2005**, *88*, 3032−3036.
(22) Park, B. K.; Kim, D.; Jeong, S.; Moon, J.; Kim, J. S. *Thin Solid Films* **2007**, *515*, 7706−7711.
(23) Luechinger, N. A.; Athanassiou, E. K.; Stark, W. J. *Nanotechnology* **2008**, *19*, 445201.
(24) Chen, S.; Carroll, D. L. *Nano Lett.* **2002**, *2*, 1003−1007.
(25) Hao, E.; Kelly, K. L.; Hupp, J. T.; Schatz, G. C. *J. Am. Chem. Soc.* **2002**, *124*, 15182−15183.
(26) Maillard, M.; Huang, P.; Brus, L. *Nano Lett.* **2003**, *3*, 1611−1615.
(27) Lu, Q.; Lee, K.-J.; Lee, K.-B.; Kim, H.-T.; Lee, J.; Myung, N. V.; Choa, Y.-H. *J. Colloid Interface Sci.* **2010**, *342*, 8−17.
(28) Meng, L.; Lu, P.; Li, S.; Zhao, J.; Li, T. *Powder Technol.* **2012**, *228*, 284−294.
(29) Roberts, J. N.; Schwartz, L. M. *Phys. Rev. B* **1985**, *31*, 5990−5997.
(30) McLachlan, D. S.; Blaszkiewicz, M.; Newnham, R. E. *J. Am. Ceram. Soc.* **1990**, *73*, 2187−2203.
(31) Tai, Y.-L.; Yang, Z.-G. *J. Mater. Chem.* **2011**, *21*, 5938−5943.
(32) Lee, H.-H.; Chou, K.-S.; Huang, K.-C. *Nanotechnology* **2005**, *16*, 2436−2441.
(33) Zhang, Z.; Zhang, X.; Xin, Z.; Deng, M.; Wen, Y.; Song, Y. *Nanotechnology* **2011**, *22*, 425601.
(34) Komoda, N.; Nogi, M.; Suganuma, K.; Kohno, K.; Akiyama, Y.; Otsuka, K. *Nanoscale* **2012**, *4*, 3418.
(35) Perelaer, J.; Smith, P. J.; Mager, D.; Soltman, D.; Volkman, S. K.; Subramanian, V.; Korvink, J. G.; Schubert, U. S. *J. Mater. Chem* **2010**, *20*, 8446.
(36) Magdassi, S.; Grouchko, M.; Berezin, O.; Kamyshny, A. *ACS Nano* **2010**, *4*, 1943.
(37) Deng, D.; Jin, Y.; Cheng, Y.; Qi, T.; Xiao, F. *ACS Appl. Mater. Interfaces* **2013**, *5*, 3839.